Journal of Science and Transport Technology
Journal homepage: https://jstt.vn/index.php/en

UNIVERSITY OF TRANSPORT TECHNOLOGY

Experimental and numerical validations of predictive models for compressive strength of pervious concrete

Van-Hung Nguyen[1], Hoang-Quan Nguyen[1], Bao-Viet Tran[1], Thai-Son Vu[2], Gun-Cheol Lee[3], Viet-Hung Vu[4,*]

[1]University of Transport and Communications, No.3 Cau Giay Street, Lang Ward, Ha Noi, Viet Nam

[2]Hanoi University of Civil Engineering, No.55 Giai Phong Street, Bach Mai Ward, Ha Noi, Viet Nam

[3]Department of Architectural Engineering, Korea National University of Transportation, Chungju, Korea

[4]Campus in Ho Chi Minh City, University of Transport and Communications, No.450-451 Le Van Viet Street, Tang Nhon Phu Ward, Ho Chi Minh City, Viet Nam

Article info
Type of article:
Original research paper

DOI:
https://doi.org/10.58845/jstt.utt.2026.en.6.3.1-20

***Corresponding author:**
Email address:
hungvv_ph@utc.edu.vn

Received: 02/12/2025
Received in Revised Form: 15/04/2026
Accepted: 29/05/2026

Abstract: Pervious concrete (PC) is a key material in sustainable urban development, but its design is complicated by the inverse relationship between permeability and compressive strength. To optimize its use, various predictive models—analytical, numerical, and data-driven—have been developed. However, a comparative validation of these diverse approaches on a consistent experimental dataset is lacking. This study aims to validate and compare the performance of three fundamental predictive frameworks: an analytical model based on micromechanics, a numerical simulation using the phase-field method, and an Artificial Intelligence (AI) approach, specifically a "white-box" symbolic regression model. An experimental case study involving the fabrication and testing of PC specimens was conducted to provide a new, independent dataset for validation. The results show that the symbolic regression, finite element method, and micromechanical models demonstrate strong agreement with the experimental data, achieving a high coefficient of determination. While black-box AI models often offer high accuracy, this study highlights that simpler, interpretable models provide a compelling balance of precision and practical applicability for engineering design.

Keywords: Pervious concrete; finite element method; compressive strength; symbolic regression; Artificial Intelligence.

1. Introduction

In recent decades, the rapid pace of urbanization has led to a significant increase in impermeable surfaces, creating pressing environmental challenges such as urban flooding and the depletion of groundwater levels. To mitigate these issues, sustainable solutions like Sustainable Urban Drainage Systems (SUDS) have been widely adopted, in which Pervious Concrete (PC) plays a pivotal role. As a special type of concrete with a high porosity of 15% to 35%, PC offers an effective method for managing stormwater while serving as a moderate load-bearing pavement surface, such as sidewalks, bicycle paths, parking lots, and light-duty roads [1–4].

The design of PC mixtures, however, presents a significant challenge compared to conventional concrete. While the primary function of standard concrete is strength, PC design must concurrently balance two conflicting properties: permeability and mechanical strength. It is widely accepted that an increase in porosity enhances permeability but leads to a substantial decrease in strength, and vice versa. Therefore, the design process often begins by selecting a target porosity, after which the compressive strength (CS) is estimated. This reliance highlights the critical need for accurate models that can predict the relationship between compressive strength, porosity, and other mixture constituents to optimize material design and ensure structural integrity. This systematic approach reduces reliance on time-consuming trial-and-error laboratory experiments [5–11].

To address the fundamental question regarding the relationship between target porosity and compressive strength, early empirical formulas were proposed to overcome the challenges posed by the material's complex structure. Accordingly, the strength-porosity relationship is typically expressed as a function of the concrete matrix strength (corresponding to zero macro-porosity) and specific empirical parameters. Literature classifies these models into three main types: linear, power, and exponential functions [5]. Building upon these basic equations, modified models have been proposed to account for specific material properties, such as aggregate size, pore size, water–cement ratio, etc. However, these semi-empirical models exhibit inherent limitations. For instance, linear regression formulas fail to capture the non-linear nature of the compressive strength-porosity relationship. At the same time, exponential and power models often struggle to predict the failure thresholds where material collapse occurs. Consequently, their applicability is frequently restricted to specific experimental datasets. A more scientifically grounded alternative is the micromechanical approach based on homogenization theory, accounting for the distinct properties of the aggregate, cement matrix, and voids [12–17]. Several theoretical formulas grounded in the micromechanical framework have been presented in the literature [18, 19] to describe the strength–porosity relationship of PC. Nevertheless, simplified models, such as those assuming a central pore, are often insufficient to account for the structural complexity of the concrete fully. Beyond standard regression laws, more complex theoretical formulas highlight that strength is not only a function of total volume of voids but is also influenced by: pore characteristics [20], solid phase interactions [21], aggregate morphology [22], etc. For example, Vu et al. [23] proposed a generalized self-consistent approximation scheme to describe the material's behavior, which aims to derive theoretical relationships from the material’s composition and microstructures. In this approach, the von Mises strain field is approximated through an averaging process, thereby establishing a link between macroscopic strength and the material's microstructural characteristics. While providing valuable physical insights, these models can be complex and often rely on geometric parameters that are difficult to ascertain in practice. More recently, the investigations have used this theory to handle unlimited components and broad volume fraction ranges, often integrating 3D X-ray CT images to create highly realistic numerical representations of the internal structure [12]. Though providing deeper insights into the material's failure mechanisms, this approach is still notably time-consuming and not available for real engineering applications.

In parallel with analytical developments, the last two decades have witnessed a paradigm shift toward data-driven methodologies, including Artificial Neural Networks (ANN), Support Vector Machines (SVM), fuzzy logic, and tree-based ensembles, etc. While traditional numerical, analytical, and regression models are often restricted to the specific boundary conditions under which they were developed, machine learning (ML) models can handle the complex, multifactorial, and nonlinear interactions inherent in PC [3, 11, 24–26]. Among these, ANN and Extreme Gradient Boosting (XGB) were singled out for their superior predictive fidelity. For instance, a study by Le et al. [27] found that an optimized XGB model could predict CS with a high coefficient of determination (R^2 = 0.92). While ANN models are highly effective at capturing patterns and correlations in large datasets, with multilayer perceptron (MLP) networks achieving R^2 values as high as 0.98 for compressive strength and 0.97 for permeability [11]. Furthermore, recent developments have integrated nature-inspired optimization algorithms (e.g., Particle Swarm Optimization, Elk Herd Optimization, or Whale Optimization) to fine-tune ML hyperparameters, further enhancing predictive stability and generalization [28]. It can be identified that data-driven methodologies offer several advantages, such as non-destructive estimation, multi-objective optimization, feature interpretability, etc. This transition is primarily driven by the limitations of traditional analytical models, which often yield lower accuracy when applied to different material types or project contexts [25]. However, the practical adoption of these algorithms is often hindered by their "black-box" nature and high computational demands. Engineers typically prioritize transparency and ease of application, qualities that opaque computational mappings fail to provide.

Conversely, "white-box" statistical regression methods offer the desired interpretability but often lack the flexibility to accurately model the complex, non-linear behavior of heterogeneous materials. To bridge the gap between predictive accuracy and interpretability, Symbolic Regression (SR) has emerged as a compelling alternative. Unlike traditional regression, which fits parameters to a pre-defined equation, SR operates within an open mathematical space, simultaneously searching for both the optimal functional form and its coefficients. This characteristic makes SR distinctively suitable for constitutive modeling, where underlying physical laws are not fully established [29]. Recent advancements in Genetic Programming-based Symbolic Regression (GPSR) have further solidified its potential in materials science [30, 31]. While standard AI frameworks like Bayesian networks or AI Feynman have their merits, GPSR has demonstrated a favorable balance between accuracy and mathematical parsimony in predicting concrete strength [32, 33]. Nevertheless, a critical gap remains in the literature: few studies rigorously evaluate whether the derived equations achieve optimal efficiency—balancing the complexity of the solution against its predictive effectiveness. This trade-off is highlighted in recent comparative work by Le et al. [27], which showed that while optimized XGB models achieve remarkable precision (R^2 = 0.92), they lack transparency. In contrast, GP-based approaches yield explicit, physically interpretable formulas with nearly comparable accuracy (R^2 = 0.90) that relate CS to key mixture parameters, offering a practical tool for engineers streamlining the mix design procedure [34]. It could be found that GPSR stands out by providing a direct, interpretable bridge between raw experimental data and the underlying physical relationships governing concrete strength, particularly for predicting the compressive strength of complex cementitious composites like PC or steel fiber-reinforced concrete, etc.

Complementing analytical formulas and AI algorithms, numerical structural modeling based on Finite Element Methods (FEM) and Discrete Element Methods (DEM) represents a critical third pillar in predictive approaches that bridges the gap between empirical observations and theoretical understanding. From a computational perspective, numerical models are particularly effective for characterizing damage properties as they offer robustness, flexibility, and detailed insights into the composite behavior. While numerical investigations on normal Portland cement concrete are extensive, modeling efforts for PC remain limited due to its complex skeleton-pore structure and the significant size disparity between aggregate particles and the thin cement paste film [35–37, 12]. Numerical models complement the above approaches by providing scientific grounding, explaining why a specific mix design fails. For instance, simulations show that as porosity increases from 15% to 25%, the failure mode shifts from aggregate fracture to ITZ debonding and mortar cracking, providing engineers with clear targets for material optimization [21]. DEM is particularly suited for PC because it treats the material as an assembly of discrete particles, mimicking its true physical composition. Typically, researchers use parallel-bond (contact constitutive) models to simulate the cementation between aggregates, and use the Particle Flow Code (PFC) framework to monitor bond failures between discrete aggregate and paste particles [20], or 3D DEM simulations to reveal the skeleton insights of aggregates in resisting compression and force transmission [37], etc.

Alternatively, FEM frameworks have been adapted to study PC, often by simplifying voids as circular inclusions within a homogeneous medium. A significant limitation of these early FEM models is the geometric discrepancy between the idealized computational domain and the actual random structure of the material. Traditional "solid modeling" often fails to represent PC's unique void structure, necessitating more specialized approaches. Recent research [12] has introduced AI-supported image processing to create highly realistic 3D FE models. By processing high-resolution scans of concrete sections, researchers can accurately map the actual positions of voids, aggregates, and even reinforcement fibers within a model. For computational efficiency, 2D Meso-scale models are frequently used to predict peak loads and analyze failure patterns by randomly generating aggregate shapes and pores using Monte Carlo methods [20, 21]. Meanwhile, Nguyen et al. [38] proposed using the Phase-Field method to simulate crack initiation and propagation within the complex pore structure of PC. This method allows for a detailed analysis of how porosity influences fracture patterns without the need for complex re-meshing. However, the high computational cost and the difficulty of accurately reconstructing the mesostructure persist as significant hurdles.

Based on this review, current methodologies for modeling PC damage can be categorized into three primary directions: analytical/semi-analytical models, artificial intelligence models, and numerical models based on damage mechanics. Despite the considerable progress within each of these approaches, a comparative validation of these diverse models against a consistent, independent experimental dataset is still lacking. Consequently, the primary objective of this paper is to evaluate the efficacy of these approaches through a comparative validation against experimental results. Section 2 introduces the theoretical frameworks of each method, with updates to the FEM approach for compressive loading. Section 3 details the experimental benchmark conducted to assess model performance, while Section 4 presents model validation using experimental data from literature and experimental tests, offering insights to guide researchers and engineers in selecting the most appropriate tools for the design and analysis of PC. Finally, conclusions and recommendations are presented.

2. Comparative modeling frameworks for pervious concrete

To predict the mechanical properties of

pervious concrete (PC), particularly the relationship between its compressive strength and porosity, three fundamental approaches have been established in the literature: analytical methods based on micromechanics, numerical simulations of failure, and data-driven Artificial Intelligence (AI) models. This section provides a brief overview of the theoretical basis of each approach.

2.1. Analytical Approach Based on Micromechanics

The micromechanical approach models pervious concrete as a multi-component composite material and uses homogenization techniques to derive its macroscopic properties from the characteristics of its constituent phases (e.g., aggregate, cement paste, and pores). This method is rooted in the concept that the failure of the entire material is governed by the failure within its individual phases.

The failure is described by a von Mises-type criterion based on phase-averaged quadratic stresses. From this, a general formula for the homogenized uniaxial compressive strength (S^e) of a multi-component brittle material can be derived:

$$S^h = \min_{\beta=a,p,cm}(S_\beta(-\frac{\mu_\beta^2}{v_\beta}(\frac{1}{3}\frac{\partial\left(\frac{1}{k^e}\right)}{\partial(\mu_\beta)}+\frac{\partial(\frac{1}{\mu_e})}{\partial(\mu_\beta)}))^{-\frac{1}{2}}) \quad (1)$$

where for each phase β (a – aggregate, cm – cement paste, p – pore), S_β is its uniaxial strength, k_β, μ_β is its shear modulus, and v_β is its volume fraction. The terms k^e and μ^e represent the homogenized bulk and shear moduli of the composite, respectively, which are typically estimated using self-consistent approximation schemes that account for phase interactions [39].

By simplifying PC into a two-phase (matrix and pores) or three-phase (aggregate, paste, and pores) system, this framework provides a powerful semi-empirical tool for relating strength to porosity, which shows a strong correlation with experimental data when its geometric parameters are properly calibrated.

2.2. Numerical Approach Using the Phase-Field Method

The numerical approach employs the finite element method (FEM) to simulate the complex fracture process in heterogeneous materials like PC. Among various techniques, the phase-field method has proven to be particularly effective for modeling crack initiation and propagation without the need for complex remeshing algorithms [40, 41]. The core idea of this method is to regularize a sharp crack surface (Γ) into a diffuse damage zone, which is described by a continuous scalar variable d(x), known as the phase field. This variable ranges from d = 0 for an undamaged material to d = 1 for a fully broken state. The total energy (E) of a body is expressed as a sum of the elastic strain energy and the fracture energy, and can be defined by:

$$E = \int_{\Omega/\Gamma} \psi_e(\varepsilon)d\Omega + \int_{\Gamma_t} g_1 dS + \int_{\Gamma_c} g_2 dS \quad (2)$$

where ψ_e is the elastic energy density, $\varepsilon = 1/2(\nabla u + \nabla u^T)$, g_1, g_2 are respectively the fracture energy in tension and crushing energy in compression. Within the regularized framework, with the introduction of the crack density function $\gamma_{d_1}(d_1,\nabla d_1)$, $\gamma_{d_2}(d_2,\nabla d_2)$ for tensile damage and compressive damage, respectively, the fracture energy can be approximated as follows:

$$\int_{\Gamma_t} g_1 dS = \int_{\Omega} g_1\, \gamma_{d_1}(d_1, \nabla d_1) d\Omega \quad (3)$$

$$\int_{\Gamma_c} g_2 dS = \int_{\Omega} g_2\, \gamma_{d_2}(d_2, \nabla d_2) d\Omega \quad (4)$$

where the crack density function can be expressed as:

$$\gamma_{d_1}(d_1, \nabla d_1) = \frac{1}{2l_1} d_1^2 + \frac{l_1}{2} \nabla d_1 . \nabla d_1 \quad (5)$$

$$\gamma_{d_2}(d_2, \nabla d_2) = \frac{1}{2l_2} d_2^2 + \frac{l_2}{2} \nabla d_2 . \nabla d_2 \quad (6)$$

where l_1, l_2 are model parameters that control the width of the smooth approximation of the crack. This approach, when combined with Monte Carlo simulations to generate realistic mesostructures of

PC, allows for the robust prediction of compressive/flexural damage behavior and fracture patterns [38].

To distinguish between the effects of tensile cracking and compressive crushing, the elastic strain energy density ψ_e is decomposed into tensile (ψ_e^+) and compressive (ψ_e^-) parts using spectral decomposition of the strain tensor. The degraded elastic energy is then given by:

$$\psi_e(\varepsilon, d_1, d_2) = [g(d_1)\psi_e^+(\varepsilon) + g(d_2)\psi_e^-(\varepsilon)] \quad (7)$$

where $g(d) = (1-d)^2 + \kappa$ is the degradation function, with $\kappa \ll 1$ being a stability constant. The evolution of the damage fields and the displacement field is determined by minimizing the total potential energy, leading to a coupled system of equations:

Mechanical Equilibrium:

$$\nabla \cdot \sigma = 0, \quad \text{with } \sigma = \frac{\partial \psi_e}{\partial \varepsilon} \quad (8)$$

Phase-Field Evolution:

$$\left(\frac{2l\mathcal{H}}{g_c} + 1\right) d - l^2 \Delta d = \frac{2l\mathcal{H}}{g_c} \quad (9)$$

Here, $\mathcal{H}$ represents the history variable, defined as the maximum value of the specific energy part attained over time to ensure the thermodynamic irreversibility of the fracture process (i.e., d can only increase). The parameters g_1 and g_2 correspond to the fracture toughness in tension ($G_{c,t}$) and crushing ($G_{c,c}$), respectively, serving as the material threshold for damage initiation.

The model is applied to a high-resolution mesh of pervious concrete, featuring aggregate and mortar phases. The Fig. 1 illustrates the 2D mesostructure used in the simulation, where the distinct phases (aggregate, mortar, and pore) are represented with the material parameters are defined as follows: the Young's moduli for the aggregate and mortar are 60 GPa and 30 GPa, respectively, with a Poisson's ratio of 0.24 for both, and the porosity for the sample is set at 19.8%. The effects of two critical parameters—length scale and fracture toughness—on the damage state are illustrated in Figs. 2 and 3. Accordingly, smaller values of the length scale lead to more localized damage but require finer meshes to ensure convergence. Conversely, higher fracture toughness of the mortar, as expected, enhances the material's resistance to failure.

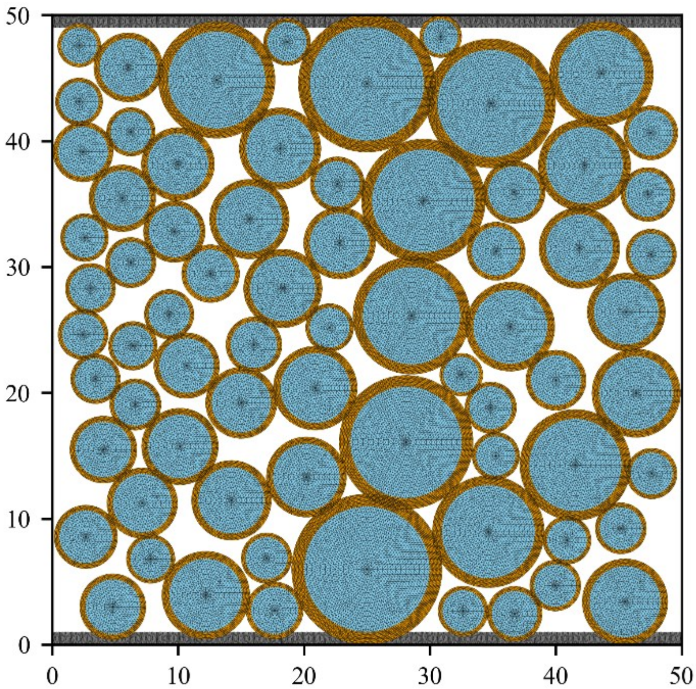

Fig. 1. FEM mesh of the pervious concrete specimen showing heterogeneous phases

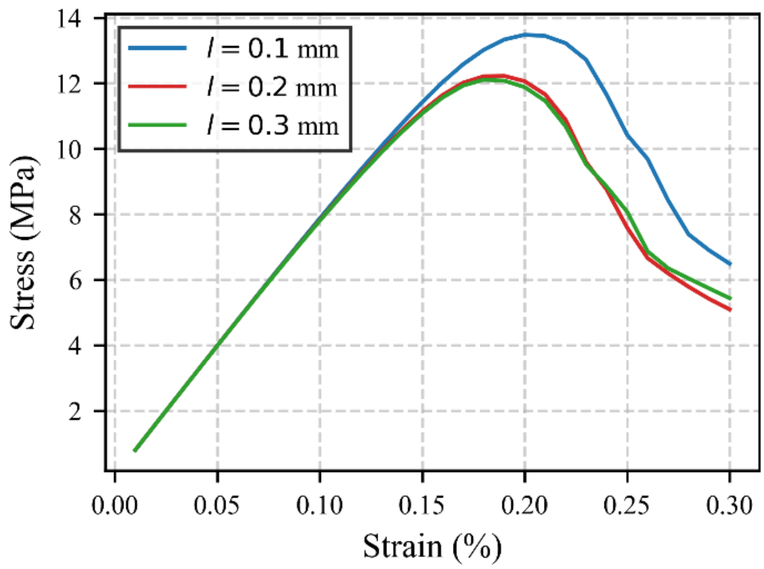

Fig. 2. Stress-strain response comparison for different values of length scale l *($l = 0.1, 0.2, 0.3$).*

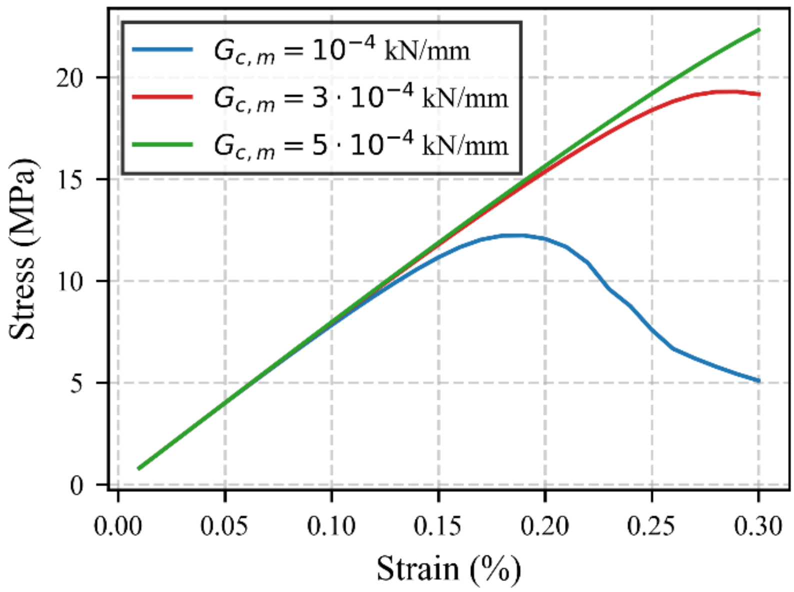

Fig. 3. Influence of mortar fracture energy $G_{c,m}$ on the compressive behavior.

2.3. Artificial Intelligence (AI) Approach

AI methods leverage machine learning algorithms to learn the complex, non-linear relationships between the mixture proportions of PC and its mechanical properties directly from experimental data. These methods can be broadly classified into two categories:

Black-Box Models: These models, including Artificial Neural Networks (ANN), Support Vector Machines (SVM), and ensemble methods like Extreme Gradient Boosting (XGB), are known for their high predictive accuracy [42]. The XGB model, an advanced decision-tree-based algorithm, constructs a highly accurate predictor by sequentially adding weak learners. It is particularly effective for structured data, achieving a high coefficient of determination ($R^2 = 0.92$) in predicting the compressive strength of PC. While powerful, the internal logic of these models is opaque, making them difficult to interpret.

White-Box Models (Symbolic Regression): In contrast, white-box models aim to find explicit mathematical formulas that are both accurate and interpretable. Genetic Programming (GP) is a leading technique in this area, which mimics the process of natural evolution to discover an optimal functional form to describe a dataset. The resulting solutions are represented as tree structures composed of mathematical functions and variables. For instance, a GP-based approach successfully derived the following simple formula to predict the compressive strength (CS) of PC with high accuracy (R^2=0.89) [34]:

$$\mathrm{CS} = 189 - 113\log(\mathrm{WC} + \log(\mathrm{AS} + \mathrm{EP}) + 1) \quad (10)$$

where WC is the water-to-cement ratio, AS is the aggregate size, and EP is the effective porosity. The simplicity and transparency of such formulas make them highly attractive for direct application in engineering design procedures.

3. Experimental test

To investigate the compressive strength of PC, considering the influence of key material properties such as aggregate size, porosity, and binder content, three mix ratios were designed with the ratio of water/cement and aggregate/cement of 0.3 and 3.5 - 4.8, respectively, based on recommendations of ACI 522R-10, ACI PRC-522-23 with a designed porosity of 10-20% [43, 44]. In these mixes, the Ordinary Portland cement was used as a binder with a density of 3.15 kg/m^3, and a poly-carboxylate high-range water reducing admixture (Flowmix 3000S, produced by Dongnam Co., Ltd. in South Korea) was applied to obtain reasonable workability of the fresh concrete. Moreover, two amounts of cement were used at 341 and 431 kg/m^3, respectively, while the superplasticizer (SP) was also used at a constant dosage of 1% by cement mass.

In this experiment, coarse aggregates with a specific gravity of 2.76, water absorption of 0.8%, and fine aggregates with a specific gravity of 2.64 were used to prepare PC samples. To introduce the different porosity for the mixture and the size affect of the aggregate particles, various aggregate sizes were considered as following: 100% aggregate particle size of 4.75 – 9.5 mm (D4.75–9.5); 80% aggregate (D4.75–9.5) + 15% aggregate particle size of 2.36 – 4.75 mm (D2.36–4.75) + 5% sand; and 50% aggregate (D4.75–9.5) + 45% aggregate (D2.36–4.75) + 5% sand as presented in Fig. 4. The designed mix proportions of PCs were presented in Table 1.

(a) (b) (c)

Fig. 4. Aggregates used in this experiment (a) D4.75–9.5, (b) D2.36–4.75, (c) sand

Table 1. Mix proportions of PCs in this experiment (kg/m^3)

Cement (C)	Water (W)	D4.75-9.5	D2.36-4.75	Sand	SP	W/C	A/C	Note
431	129	764	687	76	4.31	0.3	3.5	Mix 1
431	129	1.222	229	76	4.31	0.3	3.5	Mix 2
341	102	1.625	0	0	3.41	0.3	4.8	Mix 3

Three cylinder specimens with D100 mm × H200 mm were prepared for each mixing ratio, then their porosity according to ASTM C1754/C1754M - 25 [45] and compressive strength according to ASTM C39/C39M-24 [46] were measured at the age of 28 days. The typical specimen preparation for measuring porosity and compression test is shown in Figs. 5 and 6, respectively. Furthermore, the results obtained were presented in Table 2. It can be found in Table 2 that even though the obtained experimental results remain within the typical strength range of PC and reasonably capture the relationship between compressive strength and porosity [9, 44, 47], improvements in specimen preparation and testing procedures should be carefully considered and implemented in future experiments to obtain more consistent results with reduced variability.

(a) (b)

Fig. 5. Porosity test (a) typical specimen, (b) porosity (air void) testing

(a) (b)

Fig. 6. Compression test (a) typical specimen, (b) specimen fracture

Table 2. Experimental results obtained in this research

Specimen/Mix	Porosity (%)	Compressive strength (MPa)
Mix 1_1	10.4	20.8
Mix 1_2	9.7	17.6
Mix 1_3	10.0	16.9
Average of Mix 1	10.0	18.4
Mix 2_1	9.8	16.8
Mix 2_2	13.7	13.8
Mix 2_3	11.8	15.3
Average of Mix 2	11.2	16.3
Mix 3_1	19.9	11.5
Mix 3_2	20.7	10.7
Mix 3_3	21.3	10.3
Average of Mix 3	20.6	10.9

Table 3. Experimental data in Zhong et al. [48] and modeling results (unit of strength is MPa)

Sample	S_{cm}	$\frac{v_a}{v_{cm}+v_a}$	v_p	$S^h(Exp.)$	$S^h(Prd.)$	R^2
UHSM-2.5-1.19		0.62	0.2	65.8	63.39	
UHSM-3.0-1.19		0.66	0.25	52.9	39.3	
UHSM-3.5-1.19		0.7	0.29	42.3	19.64	
UHSM-2.5-2.38		0.62	0.21	47.5	57.78	
UHSM-3.0-2.38	174	0.66	0.27	31.7	28.88	0.47
UHSM-3.5-2.38		0.7	0.31	21.5	12.97	
UHSM-2.5-4.75		0.62	0.22	34.9	50.25	
UHSM-3.0-4.75		0.66	0.27	23.4	29.33	
UHSM-3.5-4.75		0.7	0.3	14.6	15.83	
HSM-2.5-1.19		0.57	0.24	23.4	23.55	
HSM-2.0-1.19		0.61	0.3	14.4	12.72	
HSM-3.5-1.19		0.65	0.32	10.6	8.54	
HSM-2.5-2.38		0.57	0.23	22.9	24.26	
HSM-2.0-2.38	61	0.61	0.3	12.9	12.5	0.95
HSM-3.5-2.38		0.65	0.33	8.6	7.28	
HSM-2.5-4.75		0.57	0.26	18.1	19.44	
HSM-2.0-4.75		0.61	0.3	11.3	11.57	
HSM-3.5-4.75		0.65	0.32	9.1	9.26	
NSM-2.5-1.19		0.55	0.17	23.2	23.03	
NSM-3.0-1.19		0.6	0.27	12.4	12.19	
NSM-3.5-1.19		0.63	0.31	8.4	8.31	
NSM-2.5-2.38		0.55	0.22	17.6	17.13	
NSM-3.0-2.38	29	0.6	0.28	11.5	11.29	0.99
NSM-3.5-2.38		0.63	0.32	7.5	7.58	
NSM-2.5-4.75		0.55	0.23	16	15.69	
NSM-3.0-4.75		0.6	0.29	10.5	10.45	
NSM-3.5-4.75		0.63	0.3	8.8	9.17	

4. Validations

4.1. Model validation using experimental data from the literature

First, to demonstrate the effectiveness of the proposed models, we evaluate the performance of the micromechanical model in Eq (1) (noted as WSC3, corresponding to the Weighted Self-Consistent Three-phase model) against published experimental results from Zhong et al. [48] and Xie et al. [49]. In [48], the authors measured the compressive strength and porosity of 27 series of PC, combined from three levels of matrix strength (29 MPa, 61 MPa, 174 MPa), three aggregate sizes (1.19 mm, 2.38 mm, 4.75 mm), and three aggregate-to-binder weight ratios (2.5, 3.0, 3.5). In Table 3, the four left columns present experimental data, while the two right columns show the predicted results and the corresponding coefficients of determination. The effect of matrix strength on CS is illustrated in Fig. 7 for all experimental data. For the samples made of a normal strength matrix (S_{cm} = 29 MPa), the data show a linear relationship across different aggregate sizes and aggregate-to-binder weight ratios. In Fig. 7, a good agreement between the simulations and the data is obtained (R^2 = 0.99). A similar trend is observed for the high-strength matrix case (R^2 = 0.95). For the ultra-high strength matrix series, the linear correlations between porosity and concrete strength also depend on the aggregate sizes. In fact, constructing a fitting curve for only three experimental points is of limited interest. Therefore, one simulation curve for the 9 samples of the ultra-high strength matrix case is presented, and the lower R^2 value (0.47) is easily understandable. Another empirical study on the influence of the concrete matrix on the compressive strength of PC was recently conducted in [49]. Similarly, Table 4 reports the experimental and simulation results. The analysis presented in Table 4 and Figs. 8 and 9 confirms the ability of the WSC3 model to simulate the influence of cement paste strength (Fig. 8) and aggregate-to-binder weight ratios (Fig. 9) on the uniaxial compressive strength of PC. These results reflect the accuracy and efficiency of the micromechanical model when applied to specific case studies.

4.2. Validations with experimental test

The main objective of this section is to compare the experimental results with the predicted values obtained from the proposed models. Based on the data presented in Tables 1 and 2, the regression model derived from symbolic regression (Eq (10)) was calculated and reported in Table 5 for comparison with the experimental values. Subsequently, the micromechanics-based model was evaluated using Eq (1). The results are illustrated in Fig. 10, where the CS of the cement paste was assumed to be 30 MPa. Overall, the findings demonstrate that both models capture the general trend of the strength–porosity relationship and are well aligned with the experimental data. The symbolic regression model and the micromechanics model produce relatively consistent results, especially when the assumed strength of the cement paste is adjusted.

However, at a porosity of 10%, the experimental CS was observed to be lower than both the model predictions and comparable experimental studies reported in the literature. Several factors may contribute to this discrepancy:

Experimental variability and specimen preparation: At low porosity levels, the mixture is denser and more sensitive to small variations in compaction, curing, and aggregate distribution. Inhomogeneity in the paste or insufficient interlocking between aggregates can lead to premature failure.

Measurement uncertainties: Compressive testing of PC is strongly affected by specimen geometry, loading rate, and boundary conditions. Small imperfections, such as micro-cracks or void clustering, can reduce the measured strength.

Material heterogeneity: Both the regression and micromechanics models assume uniform porosity and idealized phase distribution. In practice, pores are often irregular and unevenly distributed, producing local stress concentrations that reduce strength beyond model predictions.

Cement paste strength deviation: The micromechanics model assumes a paste strength of 30 MPa, but in reality, the effective strength of the paste may be lower due to variations in water–cement ratio, incomplete hydration, or insufficient curing.

Boundary and structural effects: At low porosity, fewer but more irregular flow channels exist, and their geometry may significantly weaken the material—a feature not fully captured by homogenization or regression-based models.

Taken together, these factors suggest that PC exhibits higher sensitivity to imperfections when designed with low porosity, which can lead to underperformance compared to theoretical predictions. Experimental results for the compressive strength (CS) of PC exhibit greater variability and deviation than those of conventional concrete due to its complex, discrete internal structure [9, 22]. Unlike the continuous matrix of normal concrete, PC is characterized by a "skeleton-pore" structure where non-uniform specimen preparation often leads to a wider scattering of stress-strain data. The mechanical performance is highly sensitive to compaction effort, where identical mix proportions can result in a 25% variance in performance depending on the specific energy applied. This uncertainty is further compounded by the inhomogeneous distribution of compaction energy across the specimen, which distorts the binder coating and pore filling. Additionally, variability stems from the morphology and size distribution of aggregates, which vary significantly by origin and processing and are often not accurately represented in standard models. Analysis of broad datasets reveals a wide spread of strength values (ranging from 1.06 to 49 MPa) and numerous outliers, reflecting the inherent inconsistencies in experimental and measurement procedures across different research studies [9, 27]. This highlights the importance of considering not only average porosity but also pore distribution, curing conditions, and experimental setup when validating predictive models.

4.3. Validations with the phase-field model

Next, the numerical phase-field model was employed for this specific case study. The analysis focused on the porosity level of 20%, where the experimental data were considered more reliable and accurate. The corresponding results are presented in Figs. 11 and 12. The results indicate that at a porosity level of 20%, the predicted CS reached 11.5 MPa, which is consistent with both the experimental and theoretical values, thereby demonstrating the effectiveness of the validation.

To clarify in more detail, as shown in Fig. 11, we originally characterized the stress–strain curves based on the transition from the elastic pre-peak stage to the quasi-brittle post-peak stage. The stochastic nature of the pore distribution in PC typically complicates the derivation of a generalized law for the post-peak region. Nevertheless, the softening regime can be further detailed. It exhibits an initial stage of accelerated damage growth, transitioning into a phase where the damage variable is distributed across the entire volume. In this final stage, the softening rate decreases as the global structure engages in energy dissipation.

This behavior is further elucidated by the crack evolution illustrated in Fig. 12. The simulation model replicates the experimental mix design described in Section 2, assuming circular aggregates coated with a mortar layer. The computational parameters are defined as follows: the Young's moduli for the aggregate and mortar are 60 GPa and 30 GPa, respectively, with a Poisson's ratio of 0.24 for both. The length scale (l_0) is set at 0.2 mm, while the fracture energy $(\mathrm{G\_c})$ of the mortar for tension and compression is taken as 10^{-5} kN/mm and 5×10^{-5} kN/mm, respectively. The loading increment is sufficiently small, with $\nabla \mathrm{U} = -10^{-3}$ mm. Fig. 12 demonstrates the progressive damage evolution, starting from the pre-peak displacement ($\varepsilon = 0.0008$), reaching the peak stress at $\varepsilon = 0.0013$, and leading to the final failure states at $\varepsilon = 0.005$.

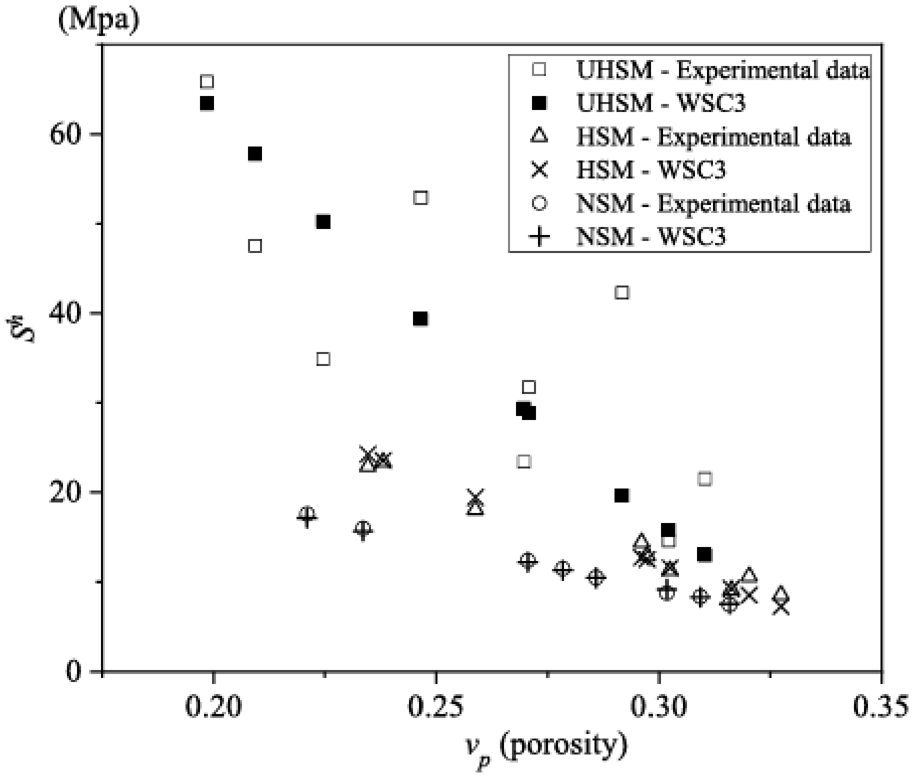

Fig. 7. Experimental data of compressive strength - porosity relationship in Zhong et al. [48] and modeling results

Table 4. Experimental data in Xie et al. [49] and modeling results (unit of strength is MPa)

Sample		$\frac{v_a}{v_{cm} + v_a}$	v_p	$S^h(\text{Exp.})$	$S^h(\text{Prd.})$	R^2
P	126.8	0.75	0.193	36.1739	33.99	0.75
	121.3	0.75	0.198	33.81	30.87	
	117.4	0.75	0.196	30.31	30.67	
	110.0	0.75	0.189	28.20	31.36	
	96.0	0.75	0.191	26.29	27.21	
	87.0	0.75	0.19	22.74	25.27	
A, T	128.6	0.74	0.201	39.05	47.35	0.75
		0.77	0.237	34.51	34.12	
		0.8	0.256	27.65	26.69	
		0.83	0.274	22.16	20.64	
		0.85	0.285	18.26	16.82	
		0.84	0.286	16.89	16.89	
		0.83	0.274	22.17	20.64	
		0.82	0.263	24.32	24.19	
		0.81	0.261	26.22	25.06	
		0.80	0.249	27.54	28.99	
		0.79	0.234	28.60	33.99	

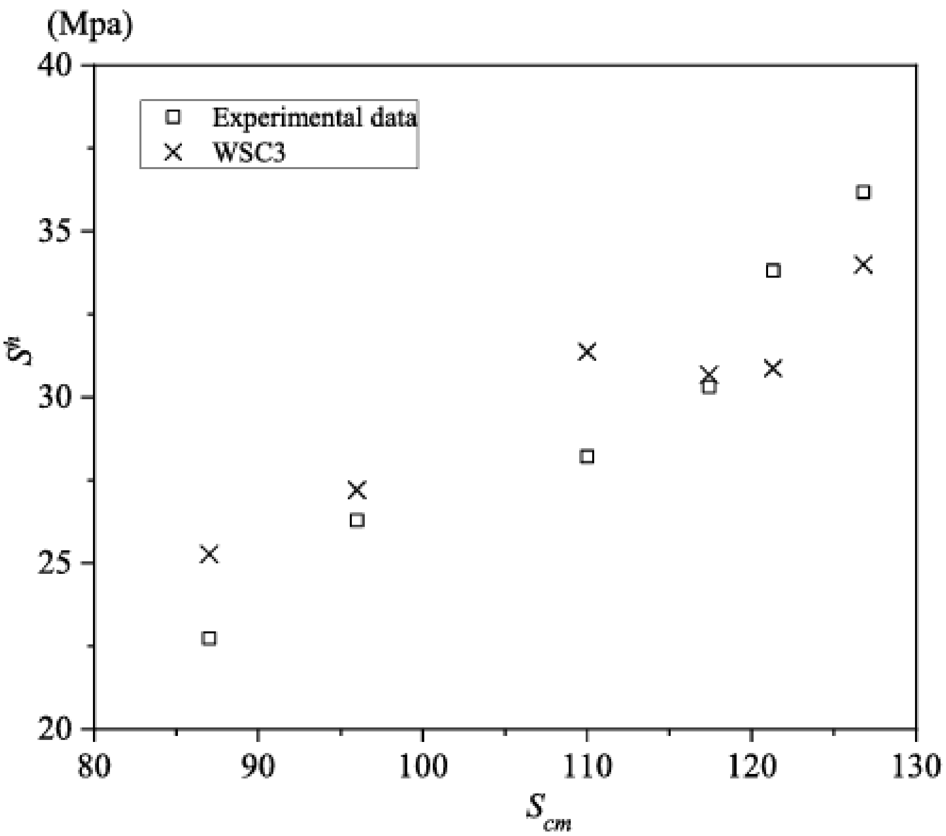

Fig. 8. Experimental data of compressive strength of pervious concrete - compressive strength of cement paste relationship in Xie et al. [49] and modeling results

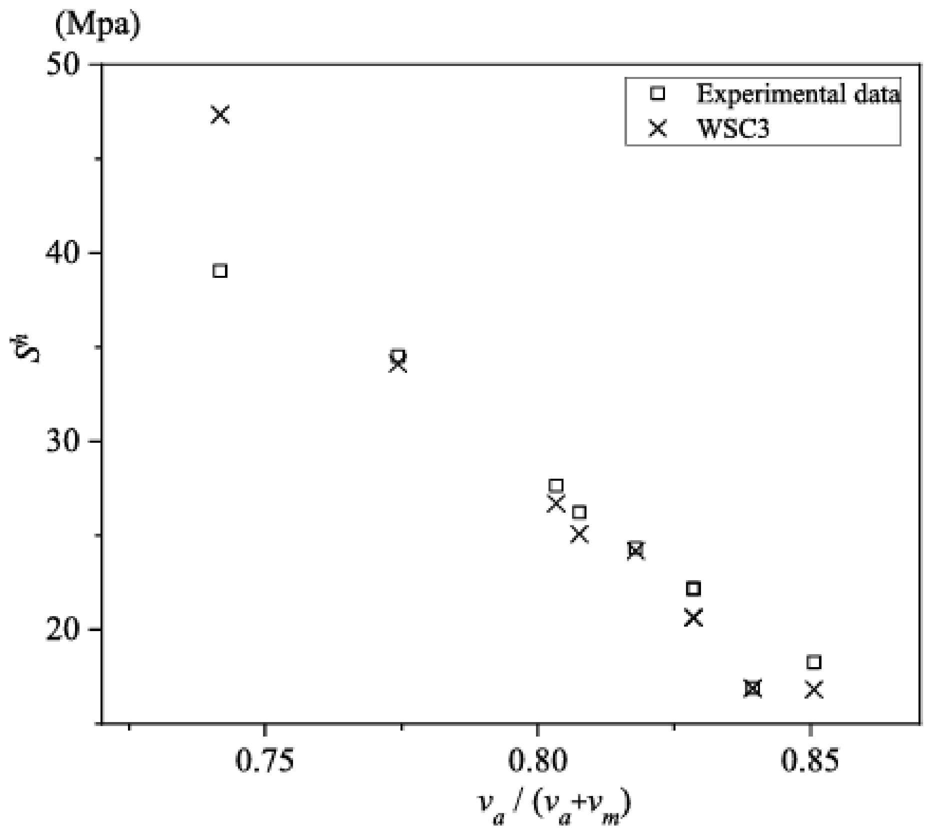

Fig. 9. Experimental data of compressive strength of pervious concrete - aggregate volume fraction relationship in Xie et al. [49] and modeling results

Table 5. Numerical results from the Symbolic regression model

Specimen /Mix	WC	AS	Porosity (%)	Symbolic regression model (MPa)	MAE (MPa)	RMSE (MPa)	SD Predicted (MPa)	SD Error (MPa)
Mix 1_1	0.3	10	10.4	23.8				
Mix 1_2	0.3	10	9.7	24.7	5.83	6.17	0.45	2.46
Mix 1_3	0.3	10	10.0	24.3				
Mix 2_1	0.3	10	9.8	24.6				
Mix 2_2	0.3	10	13.7	19.9	6.87	6.90	2.35	0.86
Mix 2_3	0.3	10	11.8	22.0				
Mix 3_1	0.3	10	19.9	14.2				
Mix 3_2	0.3	10	20.7	13.5	2.77	2.77	0.56	0.06
Mix 3_3	0.3	10	21.3	13.1				

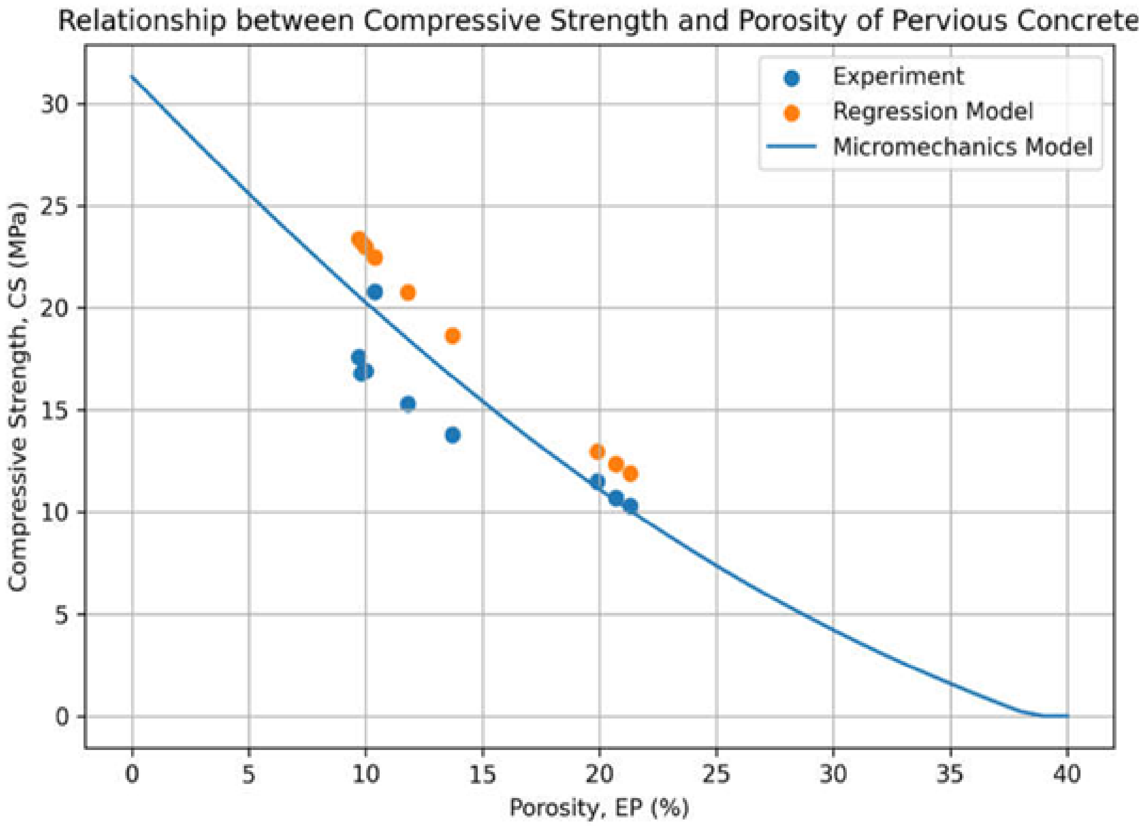

Fig. 10. Comparisons between experimental results and model predictions (symbolic regression and micromechanics) for the compressive strength–porosity relationship of pervious concrete

Based on the above discussions in this research, it can be inferred that discrepancies between physics-based and data-driven models for predicting the compressive strength (CS) of PC arise from differences in predictive accuracy, handling of non-linear interactions, and computational transparency, as briefly presented in Table 6. While data-driven models (ML/AI) offer superior precision, physics-based models (numerical/analytical) provide essential insights into material failure mechanisms that ML often lacks. Understanding the discrepancies between these methods is essential for choosing the right tool to optimize material design and ensure the structural safety of permeable pavements.

5. Conclusions

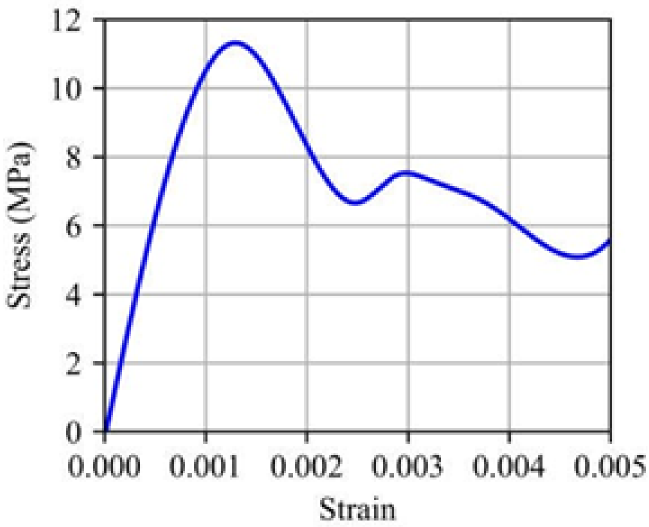

Fig. 11. Stress-strain relationship

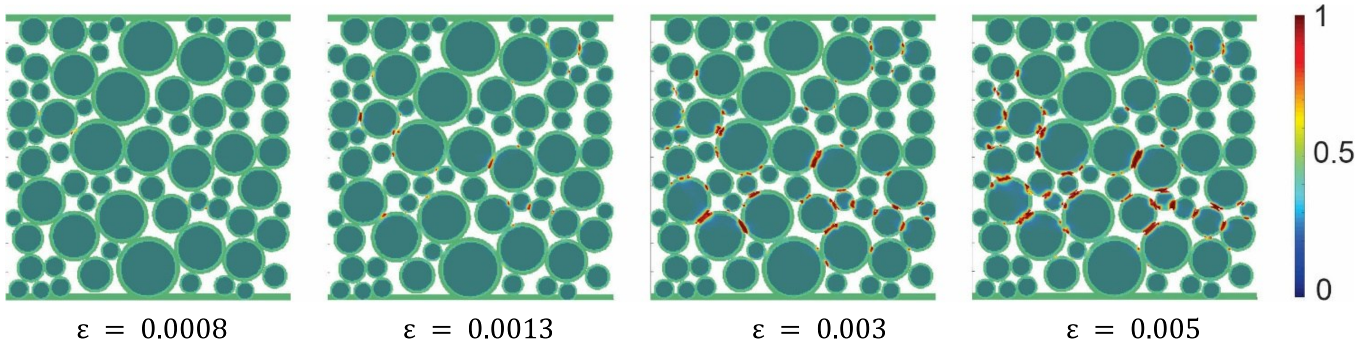

Fig. 12. Crack path evolution

Table 6. Summary of Model Capabilities

Feature	Physics-Based (Analytical/Numerical)	Data-Driven (ML/AI)
Primary Strength	Scientific grounding and physical laws [10, 21].	High predictive accuracy and pattern recognition [25].
Failure Analysis	Can simulate crack initiation and stress paths [12, 21].	Generally cannot explain how a material fails [10].
Dataset Requirement	Low; based on constitutive laws [25].	High; requires large, high-quality datasets [25].
Applicability	Often restricted to specific boundary conditions [11].	Highly adaptable to various materials/mixes [50].

This paper presented a comparative validation of three distinct predictive approaches for the compressive strength of pervious concrete: analytical micromechanics, numerical phase-field simulation, and AI-based symbolic regression. An experimental case study was performed to generate an independent dataset, against which the predictions of these models were benchmarked.

From the results, the following key conclusions can be drawn:

The AI-based symbolic regression model and the analytical micromechanical model both provided predictions that correlated strongly with the new experimental results. This finding is significant as it demonstrates that "white-box" models, which offer transparent mathematical formulas, can achieve a level of accuracy comparable to more complex or opaque methods. Their interpretability and ease of use make them highly valuable tools for practical mixture design.

The study confirms the trade-off between model complexity and applicability. While advanced numerical simulations like the phase-field method offer deep insights into failure mechanisms, and black-box AI models can yield high predictive power, their implementation can be resource-intensive. The strong performance of the simpler symbolic regression and micromechanical models, and also the finite element method, suggests they are highly efficient and suitable for routine engineering tasks.

The validation process highlighted the importance of using independent experimental data to assess the true generalization capability of predictive models. The close alignment of the selected models with the case study data enhances confidence in their use for optimizing PC mixtures.

For future work, it is recommended to expand the experimental dataset to include a wider range of aggregate types, water-cement ratios, and admixtures to further test the robustness of these models. Additionally, refining the parameters of the micromechanical model and exploring hybrid models that combine the strengths of different approaches could lead to even more powerful and reliable predictive tools for PC.

Acknowledgments

This research is funded by the Vietnam National Foundation for Science and Technology Development (NAFOSTED) under grant number 107.02-2023.15.

References

[1] B. Ferguson. (2005). Porous Pavements. 1st Edition. CRC Press. https://doi.org/10.1201/9781420038439

[2] K.S. Elango, R. Gopi, R. Saravanakumar, V. Rajeshkumar, D. Vivek, S.V. Raman. (2021). Properties of pervious concrete – A state of the art review. *Materials Today: Proceedings*, 45(Part 2), 2422–2425. https://doi.org/10.1016/j.matpr.2020.10.839

[3] R. Hari, Y. Zhuge, M.K. Madhavan. (2025). Strength enhancements and quantitative paradigms in pervious concrete: A review. *Results in Engineering*, 27, 106668. https://doi.org/10.1016/j.rineng.2025.106668

[4] X. Cai, F. Li, X. Guo, R. Li, Y. Zhang, Q. Liu, M. Jiang. (2023). Research Progress of Eco-Friendly Portland Cement Porous Concrete: A Review. *Journal of Renewable Materials*, 11(1), 103–130. https://doi.org/10.32604/jrm.2022.022684

[5] C. Lian, Y. Zhuge, S. Beecham. (2011). The relationship between porosity and strength for porous concrete. *Construction and Building Materials*, 25(11), 4294–4298. https://doi.org/10.1016/j.conbuildmat.2011.05.005

[6] A.K. Chandrappa, K.P. Biligiri. (2016). Pervious concrete as a sustainable pavement material – Research findings and future prospects: A state-of-the-art review. *Construction and Building Materials*, 111, 262–274. https://doi.org/10.1016/j.conbuildmat.2016.02.054

[7] N. Neithalath, M.S. Sumanasooriya, O. Deo. (2010). Characterizing pore volume, sizes, and connectivity in pervious concretes for permeability prediction. *Materials Characterization*, 61(8), 802–813. https://doi.org/10.1016/j.matchar.2010.05.004

[8] M.S. Sumanasooriya, N. Neithalath. (2011). Pore structure features of pervious concretes proportioned for desired porosities and their performance prediction. *Cement and Concrete Composites*, 33(8), 778–787. https://doi.org/10.1016/j.cemconcomp.2011.06.002

[9] H.A. Baseer, G.G.Md.N. Ali. (2026). Machine Learning-Based Compressive Strength Prediction in Pervious Concrete. *CivilEng*, 7(1), 3. https://doi.org/10.3390/civileng7010003

[10] S.A. Ahmad, H.U. Ahmed, S.K. Rafiq, F.S. Jafer, K.O. Fqi. (2024). A comparative analysis

of simulation approaches for predicting permeability and compressive strength in pervious concrete. *Low-carbon Materials and Green Construction*, 2, 10. https://doi.org/10.1007/s44242-024-00041-x

[11] Y. Wu, R. Pieralisi, F.G.B. Sandoval, R.D. López-Carreño, P. Pujadas. (2024). Optimizing pervious concrete with machine learning: Predicting permeability and compressive strength using artificial neural networks. *Construction and Building Materials*, 443, 137619. https://doi.org/10.1016/j.conbuildmat.2024.137619

[12] Ş. Ekmen. (2024). 3D finite element modeling of fiber-reinforced pervious concrete with novel artificial intelligence supported image processing method. *Journal of Building Engineering*, 93, 109856. https://doi.org/10.1016/j.jobe.2024.109856

[13] S. Nemat-Nasser, M. Hori. (1999). Micromechanics: Overall Properties of Heterogeneous Solids. *Elsevier*.

[14] L. Dormieux, D. Kondo, F.-J. Ulm. (2006). Microporomechanics. *John Wiley & Sons*. DOI:10.1002/0470032006

[15] B.-V. Tran, D.-C. Pham, T.-H.-G. Nguyen. (2017). Effective medium approximation for conductivity of unidirectional coated-fiber composites. *Computational Thermal Sciences*, 9(1), 63-76. DOI: 10.1615/ComputThermalScien.2017015911

[16] B.-V. Tran, D.-C. Pham. (2018). Refined polarization approximations for conductivity of isotropic composites. *International Journal of Thermal Sciences*, 131, 72–79. https://doi.org/10.1016/j.ijthermalsci.2018.05.021

[17] B.-V. Tran, D.-C. Pham, M.-D. Loc, M.-C. Le. (2019). An adaptive approach for the chloride diffusivity of cement-based materials. *Computers and Concrete*, 23(2), 145–153. https://doi.org/10.12989/cac.2019.23.2.145

[18] D. Li, Z. Li, C. Lv, G. Zhang, Y. Yin. (2018). A predictive model of the effective tensile and compressive strengths of concrete considering porosity and pore size. *Construction and Building Materials*, 170, 520–526. https://doi.org/10.1016/j.conbuildmat.2018.03.028

[19] J. Sun, J. Zhang, Y. Gu, Y. Huang, Y. Sun, G. Ma. (2019). Prediction of permeability and unconfined compressive strength of pervious concrete using evolved support vector regression. *Construction and Building Materials*, 207, 440–449. https://doi.org/10.1016/j.conbuildmat.2019.02.117

[20] L. Liao, S. Wu, R. Hao, Y. Zhou, P. Xie. (2023). The compressive strength and damage mechanisms of pervious concrete based on 2D mesoscale pore characteristics. *Construction and Building Materials*, 386, 131561. https://doi.org/10.1016/j.conbuildmat.2023.131561

[21] F. Liu, Z. Li, B. Liu, Z. Yu, Z. Li, M. Zhu, Y. Wang, X. Ding. (2025). Experimental and Numerical Investigations on the Influences of Target Porosity and w/c Ratio on Strength and Permeability of Pervious Concrete. *Materials*, 18(17), 3951. https://doi.org/10.3390/ma18173951

[22] S.H.B. Wijekoon, N. Ahilash, V. Pravinjan, K. Virupashan, N. Sathiparan, P. Jeyananthan, D.N. Subramaniam. (2025). Investigation of impact of aggregate shape on pervious concrete using machine learning classification methods. *Engineering Applications of Artificial Intelligence*, 143, 110008. https://doi.org/10.1016/j.engappai.2025.110008

[23] V.-H. Vu, B.-V. Tran, B.-A. Le, H.-Q. Nguyen. (2021). Prediction of the relationship between strength and porosity of pervious concrete: A micromechanical investigation. *Mechanics Research Communications*, 118,

103791. https://doi.org/10.1016/j.mechrescom.2021.103791

[24] S.S.A.B. Padavala, S. Avudaiappan, V. Noolu. (2025). Experimental and machine learning based analysis of pervious concrete enhanced with fly ash and silica fume. *Next Materials*, 9, 101018. https://doi.org/10.1016/j.nxmate.2025.101018

[25] N. Adsul, Y. Choi, S.-T. Kang. (2025). A Comprehensive Review of Numerical and Machine Learning Approaches for Predicting Concrete Properties: From Fresh to Long-Term. *Materials*, 18(15), 3718. https://doi.org/10.3390/ma18153718

[26] I. Nunez, A. Marani, M. Flah, M.L. Nehdi. (2021). Estimating compressive strength of modern concrete mixtures using computational intelligence: A systematic review. *Construction and Building Materials*, 310, 125279. https://doi.org/10.1016/j.conbuildmat.2021.125279

[27] B.-A. Le, V.-H. Vu, S.-Y. Seo, B.-V. Tran, T. N.-Sy, M.-C. Le, T.-S. Vu. (2022). Predicting the Compressive Strength and the Effective Porosity of Pervious Concrete Using Machine Learning Methods. *KSCE Journal of Civil Engineering*, 26(11), 4664–4679. https://doi.org/10.1007/s12205-022-1918-z

[28] M.D. Rout, D. Kar, S. Dash, B.P. Mishra. (2026). Predicting compressive strength of pervious concrete using a hybrid nature-inspired machine learning model and partial dependence plot interpretability analysis. *Progress in Engineering Science*, 3(2), 100244. https://doi.org/10.1016/j.pes.2026.100244

[29] J. Duffy, J. Engle-Warnick. (2002). Using Symbolic Regression to Infer Strategies from Experimental Data. *Evolutionary Computation in Economics and Finance*. *Studies in Fuzziness and Soft Computing, vol 100. Physica, Heidelberg. 2002, pp. 61–82.* https://doi.org/10.1007/978-3-7908-1784-3_4

[30] J.R. Koza. (1992). Genetic Programming: On the Programming of Computers by Means of Natural Selection. *Bradford Books*.

[31] M. Affenzeller, S. Wagner, S. Winkler, A. Beham. (2009). Genetic Algorithms and Genetic Programming: Modern Concepts and Practical Applications. *CRC Press*.

[32] C.-H. Lim, Y.-S. Yoon, J.-H. Kim. (2004). Genetic algorithm in mix proportioning of high-performance concrete. *Cement and Concrete Research*, 34(3), 409–420. https://doi.org/10.1016/j.cemconres.2003.08.018

[33] A. Gholampour, A.H. Gandomi, T. Ozbakkaloglu. (2017). New formulations for mechanical properties of recycled aggregate concrete using gene expression programming. Construction and Building Materials, 130, 122–145.https://doi.org/10.1016/j.conbuildmat.2016.10.114

[34] B.-A. Le, B.-V. Tran, T.-S. Vu, V.-H. Vu, V.-H. Nguyen. (2024). Predicting the Compressive Strength of Pervious Cement Concrete based on Fast Genetic Programming Method. *Arabian Journal for Science and Engineering*, 49, 5487–5504. https://doi.org/10.1007/s13369-023-08396-2

[35] R. Pieralisi, S.H.P. Cavalaro, A. Aguado. (2017). Advanced numerical assessment of the permeability of pervious concrete. *Cement and Concrete Research*, 102, 149–160. https://doi.org/10.1016/j.cemconres.2017.09.009

[36] C. Xie, L. Yuan, M. Zhao, Y. Jia. (2020). Study on failure mechanism of porous concrete based on acoustic emission and discrete element method. *Construction and Building Materials*, 235, 117409. https://doi.org/10.1016/j.conbuildmat.2019.117409

[37] J. Zhou, M. Zheng, Q. Zhan, R. Zhou, Y. Zhang, Y. Wang. (2023). Discrete element modelling of the uniaxial compression behavior

of pervious concrete. Case Studies in Construction Materials, 18, e01937. https://doi.org/10.1016/j.cscm.2023.e01937

[38] H.-Q. Nguyen, B.-V. Tran, T.-S. Vu. (2022). Numerical approach to predict the flexural damage behavior of pervious concrete. *Case Studies in Construction Materials*, 16, e00946. https://doi.org/10.1016/j.cscm.2022.e00946

[39] B.-V. Tran. (2019). A simple model to predict effective conductivity of multicomponent matrix-based composite materials with high volume concentration of particles. *Composites Part B: Engineering*, 173, 106997. https://doi.org/10.1016/j.compositesb.2019.106997

[40] T.T. Nguyen, J. Yvonnet, M. Bornert, C. Chateau, K. Sab, R. Romani, R. Le Roy. (2016). On the choice of parameters in the phase field method for simulating crack initiation with experimental validation. *International Journal of Fracture*, 197, 213–226. https://doi.org/10.1007/s10704-016-0082-1

[41] H.Q. Nguyen, B.V. Tran, B.A. Le, T.T. Nguyen. (2024). On the choice of a phase field model for describing fracture behavior of concrete. *International Journal of Computational Materials Science and Engineering*, 13(1), 2350016. https://doi.org/10.1142/S2047684123500161

[42] T. N.-Sy, M.-N. Vu, A.-D. T.-Le, B.-V. Tran, T.-T.-N. Nguyen, T.-T. Nguyen. (2021). Studying petrophysical properties of micritic limestones using machine learning methods. *Journal of Applied Geophysics*, 184, 104226. https://doi.org/10.1016/j.jappgeo.2020.104226

[43] ACI Committee 522. (2010). ACI 522R-10: Report on Pervious Concrete.

[44] ACI Committee 522. (2023). ACI PRC-522-23: Pervious Concrete—Report.

[45] ASTM. (2025). ASTM C1754/C1754M-25. Standard Test Method for Density and Void Content of Hardened Pervious Concrete. DOI: 10.1520/C1754_C1754M-25

[46] ASTM. (2024). ASTM C39/C39M-24. Standard Test Method for Compressive Strength of Cylindrical Concrete Specimens. https://doi.org/10.1520/C0039_C0039M-24

[47] N.T. Dung, N.V. Hung, (2024). Study on the influence of material composition factors on the porosityand compressive strength of perviousconcrete. *Transport and Communications Science Journal*, 75(9), 2400–2414. https://doi.org/10.47869/tcsj.75.9.13

[48] R. Zhong, K. Wille. (2016). Compression response of normal and high strength pervious concrete. *Construction and Building Materials*, 109, 177–187. https://doi.org/10.1016/j.conbuildmat.2016.01.051

[49] X. Xie, T. Zhang, C. Wang, Y. Yang, A. Bogush, E. Khayrulina, Z. Huang, J. Wei, Q. Yu. (2020). Mixture proportion design of pervious concrete based on the relationships between fundamental properties and skeleton structures. *Cement and Concrete Composites*, 113, 103693. https://doi.org/10.1016/j.cemconcomp.2020.103693

[50] G. Yu, S. Zhu, Z. Xiang. (2024). The Prediction of Pervious Concrete Compressive Strength Based on a Convolutional Neural Network, *Buildings*, 14(4), 907. https://doi.org/10.3390/buildings14040907